Landslides (2009) 6:153–159
DOI 10.1007/s10346-009-0147-6
Received: 7 November 2008
Accepted: 10 February 2009
Published online: 17 April 2009

H. P. Sato · E. L. Harp

Interpretation of earthquake-induced landslides triggered by the 12 May 2008, M7.9 Wenchuan earthquake in the Beichuan area, Sichuan Province, China using satellite imagery and Google Earth

Abstract The 12 May 2008 M7.9 Wenchuan earthquake in the People's Republic of China represented a unique opportunity for the international community to use commonly available GIS (Geographic Information System) tools, like Google Earth (GE), to rapidly evaluate and assess landslide hazards triggered by the destructive earthquake and its aftershocks. In order to map earthquake-triggered landslides, we provide details on the applicability and limitations of publicly available 3-day-post- and pre-earthquake imagery provided by GE from the FORMOSAT-2 (formerly ROCSAT-2; Republic of China Satellite 2). We interpreted landslides on the 8-m-resolution FORMOSAT-2 image by GE; as a result, 257 large landslides were mapped with the highest concentration along the Beichuan fault. An estimated density of 0.3 landslides/km^2 represents a minimum bound on density given the resolution of available imagery; higher resolution data would have identified more landslides. This is a preliminary study, and further study is needed to understand the landslide characteristics in detail. Although it is best to obtain landslide locations and measurements from satellite imagery having high resolution, it was found that GE is an effective and rapid reconnaissance tool.

Keywords Landslides · Sichuan · Wenchuan · Earthquake · Google Earth · FORMOSAT-2 · SPOT5 · Satellite

Introduction

The M7.9 Wenchuan earthquake of 12 May 2008 in east Sichuan Province of the People's Republic of China resulted in at least 69,185 fatalities. Located at 30.99°N, 103.36°E with a hypocentral depth of 19 km, it had an estimated rupture length of more than 200 km (USGS 2008). Consequently, this earthquake caused thousands of landslides covering a wide area of 285×20 km. With access to satellite data, the World Wide Web can provide such images swiftly. For example, in the case of the 2005 northern Pakistan earthquake (M7.6) GeoEye Inc. quickly published IKONOS images on their Web homepage after the earthquake showing landslides triggered by the earthquake (Une and Kumaki 2007). On 20 May 2008 Google Earth (GE) published satellite images taken on 15 May 2008, after the earthquake. In this study, we produced a preliminary map of landslides using images provided by GE and estimated their location errors, and we calculated landslide density among slope angles considering these errors using SRTM3 (Shuttle Radar Topography Mission 3)-DEM (Digital Elevation Model) at 90-m resolution, downloaded from the NASA (National Aeronautics and Space Administration) FTP site (NASA 2006).

Historical seismicity in the region

The epicenter of this earthquake is shown as "A" in Fig. 1, which also shows topography from SRTM30-DEM at 900-m resolution (NASA 2006). Historically, Sichuan Province has been damaged repeatedly by large earthquake-induced landslides.

On 1 June 1786, the Kangding–Luding earthquake (~M7.8, 20 km depth) occurred at the epicenter shown as "B" in Fig. 1 (Dai et al. 2005). According to Dai et al. (2005), the historical document written by the local governor in the Qing Dynasty indicates that the earthquake triggered many small slope failures and rock falls in and around the epicenter and the fault, and produced a landslide dam in the main channel of the Dadu River (Fig. 1). Ten days after the earthquake, the dam was broken and the ensuing flood killed approximately 100,000 people. On 25 August 1933, the M7.3 Diexi earthquake (C in Fig. 1; USGS 2008) caused landslides that blocked the Min River (Science Museum of China 2008) and destroyed the town of Diexi (Tang et al. 1994).

Study area

The study area, shown by the red rectangle in Fig. 1, is 130 km NE of the epicenter, where approximately 6 m slip at 8 km depth on the fault plane was estimated based on finite fault modeling (USGS 2008). After the earthquake, FORMOSAT-2 (formerly ROCSAT-2; Republic of China Satellite 2) images were taken of the study area.

An enlarged view of the study area is also shown in Fig. 2 with elevation data from the SRTM3-DEM. Total relief within the study area (Fig. 2a) is approximately 2,000 m. The black area at the lower left margin of the figure is an area of no data.

Method and results

The FORMOSAT-2 satellite was launched by Taiwan on 21 May 2004; it has a sun-synchronous orbit at an elevation of 891 km and passes over Taiwan twice daily. It provides black/white and color images in 2-m and 8-m resolution (Taiwan National Space Organization 2008).

On 15 May, the Taiwan Central News Agency reported the landslides near Beichuan with a FORMOSAT-2 color image (off nadir angle=ca. 37°) taken on 14 May. On 20 May, the same FORMOSAT-2 color image became available on GE and offered a relatively cloud-free view of the landslide-affected area around Beichuan which was the most devastated area of all areas affected by the earthquake. Figure 3 shows the Xinbei School landslide which buried the junior high school in Beichuan, missing at least 1,000 students and teachers (Xinhua 2008). We used the color image shown in Fig. 4a to map landslides triggered by the earthquake. The image covers approximately 3,015 km^2, within a rectangle 45 km by 67 km in east/west and north/south directions, respectively. Beichuan is located near the black square in Fig. 4a.

Landslide interpretation

Landslides triggered by the earthquake were mainly classified as rock falls and rock slides (although many of the larger failures

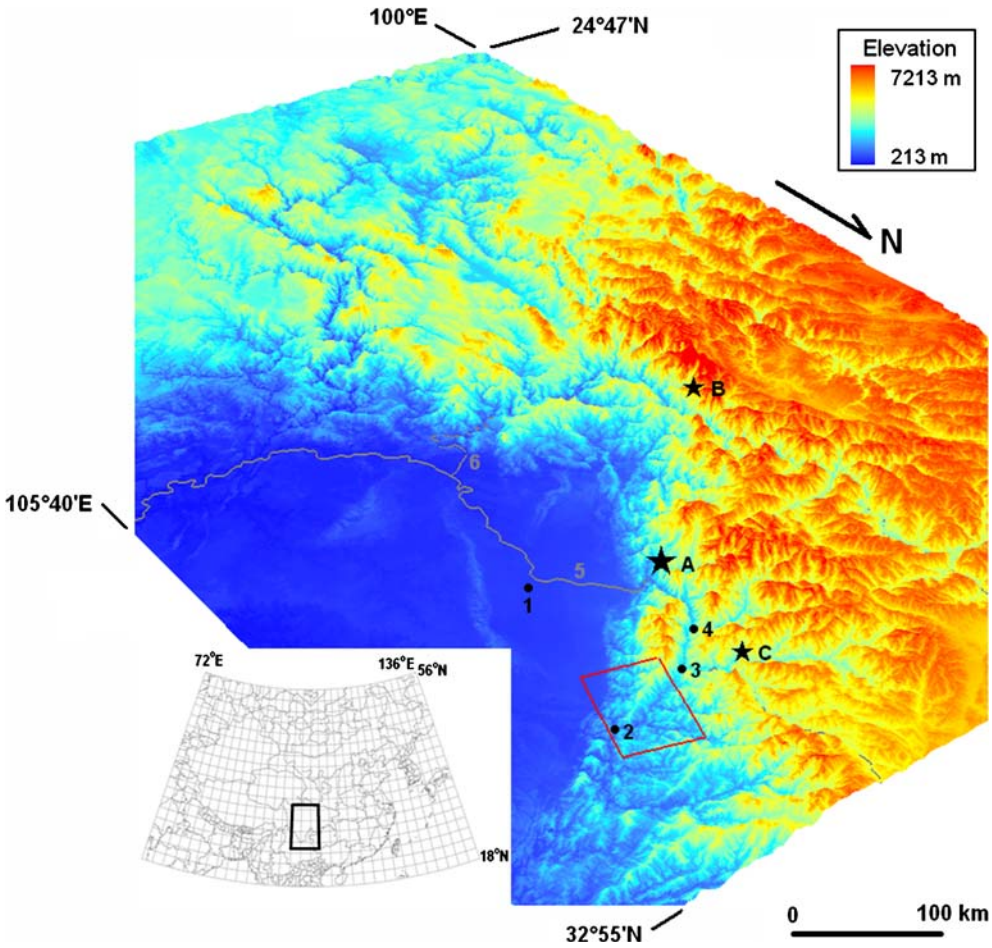

Fig. 1 Overview of the study area. **a** This M7.9 earthquake epicenter (USGS 2008), **b** epicenter of M7.8 1786 Kangding–Luding earthquake in 1786 (Dai et al. 2005), **c** the M7.3 Diexi earthquake epicenter in 1933 (USGS 2008), *1* Chengdu, *2* Beichuan, *3* Mao Xian, *4* Wenchuan, *5* Min River, *6* Dadu River. *Red frame* indicates the study area of Fig. 2

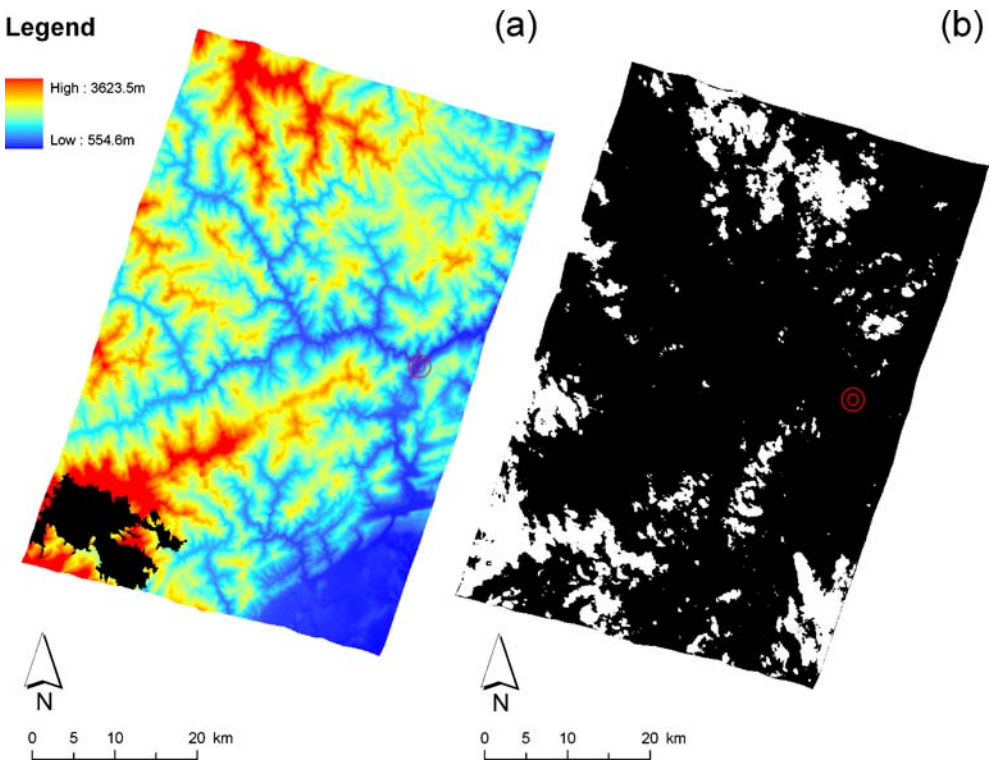

Fig. 2 Study area. *Red double circle* shows Beichuan. **a** DEM of the study area, **b** cloud and no-cloud area is shown in *white* and *black*, respectively

Fig. 3 Landslides that impacted the city of Beichuan and the Xinbei School (Xinbei School landslide). Picture was taken on 26 September, 2008

could also be classified as avalanches) with volumes commonly of several hundred thousand cubic meters. Landslides judged to be triggered by the earthquake met the following criteria observed on the satellite imagery: (1) deposits were clearly identified at the foot of the slope covering roads or other structures or extending into rivers and streams, (2) slope failures showed newly denuded vegetation on the slope, (3) slope failures had orange or bright white contrast as compared to surrounding slopes of pale brown, (4) slope failures were dark brown in contrast to the surrounding pale brown slopes, and/or (5) debris-movement paths could be clearly observed. Source locations of the landslides were plotted as red and white dots in Fig. 5a and b, respectively. The red frame shown in Fig. 5a depicts the area of concentrated landslides. Red hollow circles and black solid lines in Fig. 5b shows aftershock epicenters (USGS 2008) and fault traces (Densmore et al. 2007), respectively.

Based on our analysis, a total of 257 landslides were detected. Because of the image resolution, the smallest landslide that could be recognized should have been approximately 8×8 m. However, unless landslides had an enough large area of ca. 500×100 m, we

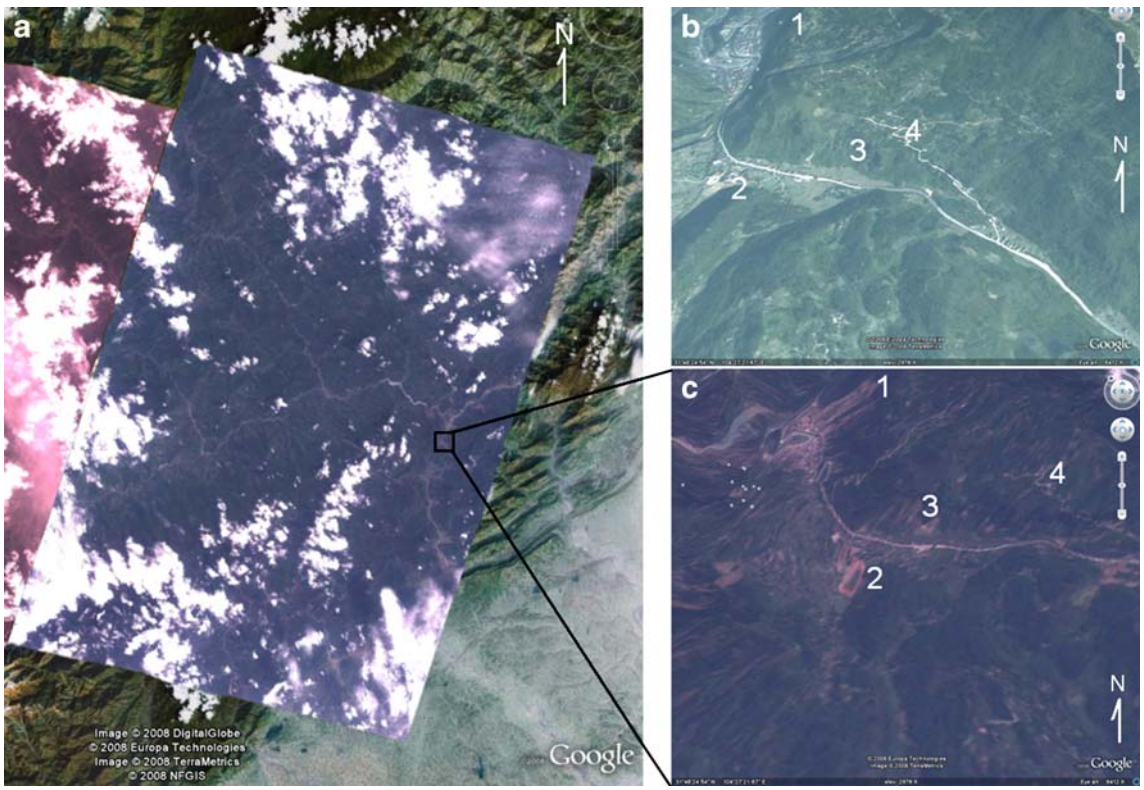

Fig. 4 **a** FORMOSAT-2 image plotted on Google™ Earth base, **b** oblique SPOT5 image taken before the earthquake, **c** FORMOSAT-2 image covering same area as (**b**). The *number* in (**b**) and (**c**) shows same points, and location in Fig. 3 shows same points as the number *1*

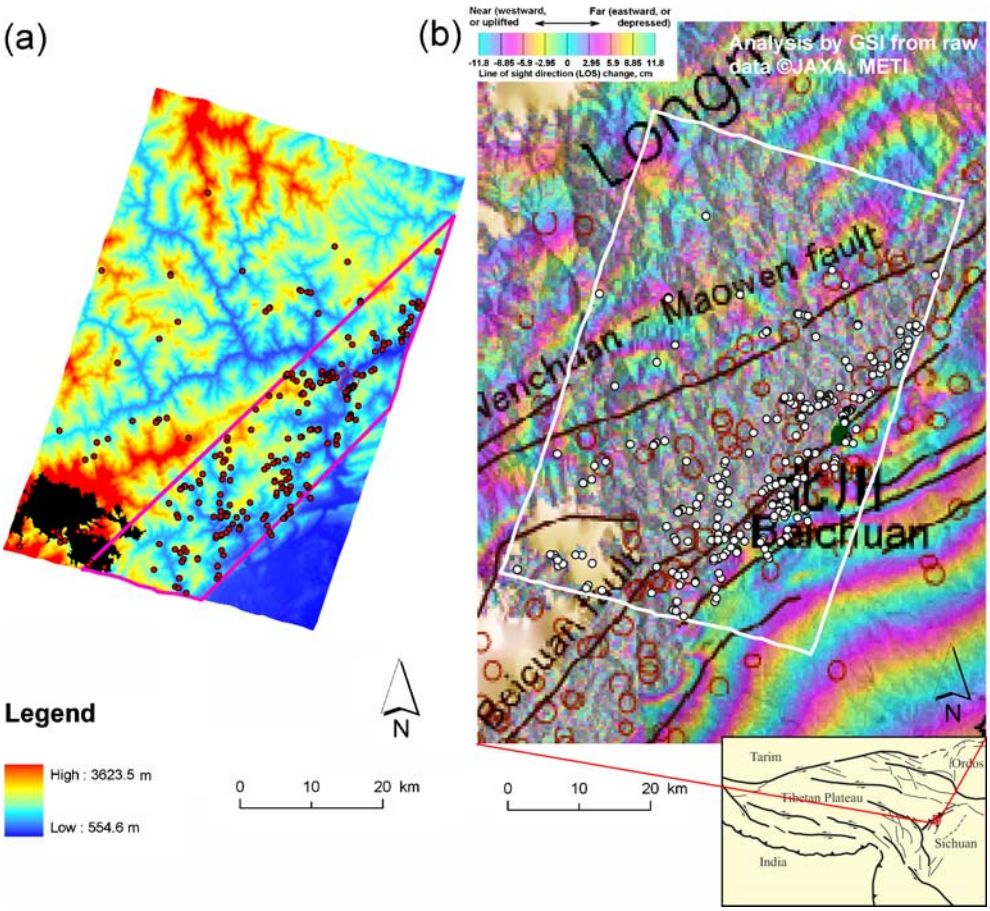

Fig. 5 **a** Interpreted landslides (*red dots*), **b** interpreted landslides (*white plots*) superimposed on the In-SAR (Interferometry Synthetic Aperture Radar) image by Geographical Survey Institute (2008) and Tobita et al. (2008). Phase-color (fringe) change indicates seismic ground deformation as shown in color index. Aftershock epicenters in *red hollow circle* and fault traces in *solid black lines* are USGS (2008) and Densmore et al. (2007), respectively. Seismotectonic setting is modified after Dong et al. (2008)

Table 1 Location error between the same landmarks on GE-DEM and SRTM3-DEM. In the table, d*E* and d*N* is the easting and northing error component calculated from (GE location) - (SRTM location)

Code	Error, d*E*(m)	Error, d*N*(m)	Error (m), $\sqrt{(dE)^2 + (dN)^2}$	Landmark	Location on SRTM3-DEM from ArcGIS	
1.	41.7	167.9	173.0	River confluence	31° 51′ 56.70″ N	104° 30′ 36.70″ E
2.	-15.7	73.1	74.7	River confluence	32° 1′ 49.58″ N	104° 34′ 39.82″ E
3.	47.7	44.8	65.4	River confluence	31° 36′ 9.96″ N	104° 12′ 51.58″ E
4.	-79.0	92.1	121.4	River confluence	31° 53′ 7.57″ N	104° 7′ 51.58″ E
5.	-189.1	284.0	341.2	Summit	31° 42′ 24.32″ N	104° 21′ 24.59″ E
6.	-99.4	391.6	404.0	Summit	32° 9′ 46.88″ N	104° 14′ 28.94″ E
7.	292.5	-107.9	311.8	Summit	32° 4′ 39.46″ N	104° 22′ 46.65″ E
8.	-95.2	47.9	106.6	Summit	31° 58′ 47.69″ N	104° 32′ 26.20″ E
9.	-58.8	10.0	59.7	Summit	31° 49′ 12.50″ N	104° 22′ 14.09″ E
10.	-68.7	-16.8	70.7	Summit	31° 44′ 35.49″ N	104° 12′ 47.26″ E
11.	-63.1	9.9	63.9	Summit	31° 46′ 29.07″ N	104° 18′ 9.93″ E
12.	-56.1	79.3	97.1	Summit	31° 50′ 11.05″ N	104° 6′ 15.16″ E
13.	-69.8	138.2	154.9	Summit	31° 57′ 46.54″ N	104° 7′ 12.96″ E
14.	-97.7	132.9	164.9	Summit	31° 58′ 32.96″ N	104° 11′ 51.05″ E
15.	-93.6	165.3	190.0	Summit	31° 55′ 36.96″ N	104° 19′ 20.96″ E
16.	-79.4	178.6	195.5	Saddle	31° 39′ 34.53″ N	104° 23′ 3.65″ E
17.	26.8	-6.5	27.6	River meander	31° 37′ 19.76″ N	104° 20′ 44.19″ E
18.	17.6	41.1	44.7	River meander	31° 50′ 40.53″ N	104° 27′ 37.42″ E
19.	-2.2	115.8	115.8	River meander	31° 55′ 37.89″ N	104° 14′ 6.66″ E
average	-38.2	96.9	146.5			

could not determine whether the landslides met this above four criteria or not. So the average mapped size of landslide is ca. 500 × 100 m. For this reason, many smaller landslides were not mapped in the study area.

Average landslide spatial density

To calculate landslide density (landslides/km^2), we measured the cloud-free area of the FORMOSAT-2 image where landslides were mapped. We enlarged the FORMOSAT-2 image at full screen size of the 20-in. monitor, then duplicated the FORMOSAT-2 image at 90-m resolution. Next, we changed this color image into 256 shades of gray scale image data. Furthermore, we changed it into black-and-white image using the threshold pixel value of 254, 250, 240, 230, 220, 210, 200, and 190. Therefore, we obtained eight kinds of black-and-white image data. Comparing the eight images, we found that the threshold of 200, in other words, the area which the pixel value less than 200 was cloud free and suitable for landslide interpretation. Then, we were able to calculate an average landslide spatial density of 0.1 landslides/km^2.

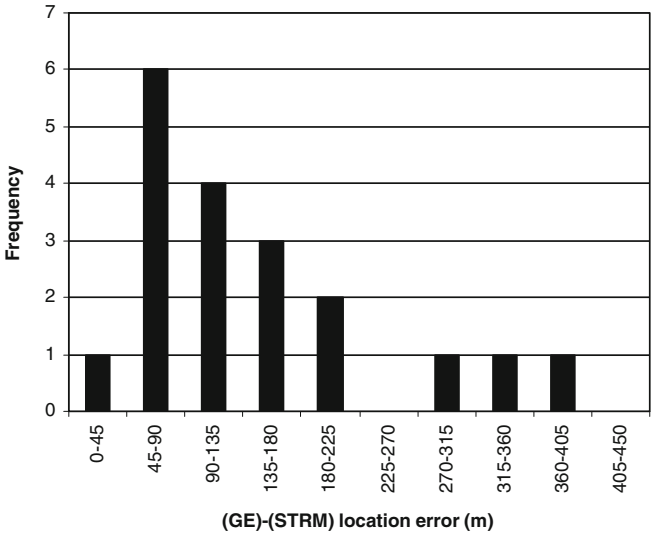

Fig. 6 Frequency plot of data in Table 1

Discussion

Landslide distribution

The landslide locations shown in Fig. 5a are concentrated in the southeast portion of the image. The Geographical Survey Institute of Japan (GSI 2008; Tobita et al. 2008) analyzed ALOS (Advanced Land Observing Satellite)/PALSAR (Phased Array type L-band Synthetic Aperture Radar) data and constructed an In-SAR (Interferometry Synthetic Aperture Radar) image. Figure 5b shows an overlay of the landslide distribution (white dots) on the In-SAR image (path 473 data, taken on 18 February 2008 and 20 May 2008).

An active microwave device, SAR, is capable of recording the electromagnetic echo backscattered from the ground surface and of arranging as a 2D image map, whose dimensions are the sensor-target distance (line of sight direction, LOS) and the platform flight direction (Colesanti and Wasowski 2006). The PALSAR sensor uses an L-band microwave (wave length=23.6 cm) that is able to penetrate leaves and tree branches. Therefore, any ground deformation obscured by plants is thought to be more detectable than with the shorter wavelength of microwave. The PALSAR sensor adopted a phased array type antenna that is a group of antennas in which the relative phases of the respective signals feeding the antennas are varied in such a way that the effective radiation pattern of the array is reinforced in a desired direction and suppressed in undesired directions. Interferometric processes between pre- and post-earthquake SAR images make it possible to detect any LOS changes caused by crustal deformation. Figure 5b shows the interferogram expressed in phase-color (fringe) change on the ALOS ascending orbit. Direction of view is from west to east; it shows only seismic surface deformation because any topographic phase contribution was retrieved using the DEM. When there is no deformation on the ground surface, the color does not change; however, when there is any deformation on the ground surface, interference colors can be perceived. In Fig. 5b, landslides are also concentrated on the color-phase area where interferometric process does not work because of the great surface disturbance due to the deformation caused by fault displacement.

GSI (2008) revealed that the boundary where the phase colors are drastically changed on the In-SAR image is along Beichuan fault (Densmore et al. 2007) near Beichuan and suggested that the boundary corresponds to the surface rupture fault. Furthermore,

Table 2 Location error between the same landmarks on FORMOSAT-2 and SPOT5

Error (m), $\sqrt{(dE)^2 + (dN)^2}$	Landmark	Location on SPOT5 image read from GE	
1,145	River meander	31° 45′ 21.75″ N	104° 16′ 14.24″ E
975	River meander	31° 48′ 13.31″ N	104° 10′ 2.17″ E
727	Road intersection	31° 50′ 3.04″ N	104° 13′ 2.63″ E
1,541	Road curve	31° 49′ 48.68″ N	104° 28′ 25.67″ E
784	Road intersection in valley bottom	31° 43′ 19.10″ N	104° 26′ 57.56″ E
1,434	Road curve	32° 1′ 26.59″ N	104° 10′ 52.56″ E
1,137	Road curve	31° 55′ 7.73″ N	104° 13′ 8.83″ E
867	Road intersection in valley bottom	31° 56′ 55.91″ N	104° 16′ 11.16″ E
906	Road curve in valley bottom	31° 53′ 54.88″ N	104° 15′ 20.22″ E
870	Road curve in valley bottom	31° 41′ 7.39″ N	104° 16′ 45.25″ E
1,038.6 (average)			

Tobita (2008) stated that the boundary is also visible near the Pengguan fault (Densmore et al. 2007; shown in SE of Beichuan in Fig. 5b); i.e., it looks like a step-over of the surface rupture fault. Field survey by Dong et al. (2008) revealed that eastward-thrusting surface rupture resulted in 2.7 m of vertical displacement in Beichuan with the vertical offset of ca. 0.8 m in a river bed in the Pengguan fault (Dong et al. 2008 call it "Guanxian–Anxian fault") zone, which was also activated by the earthquake.

Figure 5b also shows that many landslides are along the Beichuan fault. Dong et al. (2008) interpreted post-earthquake aerial photographs in the Beichuan area and traced two subsidiary fault ruptures. They mapped large landslides and also showed that landslides are located along the surface rupture. Furthermore, Fig. 5b shows that they seem to be concentrated within a 10-km-wide zone centered on the fault trace. The landslide density in this concentrated area is 0.3 landslides/km^2. In the case of the 2005 northern Pakistan earthquake, the landslide density was 3.2 landslides/km^2, which was interpreted using 2.5-m-resolution SPOT5 (System Pour l'Observation de la Terre 5) images (Sato et al. 2007). If higher resolution satellite images were available for this study area and the smaller landslides were mapped, we strongly suspect that a higher landslide density would be obtained.

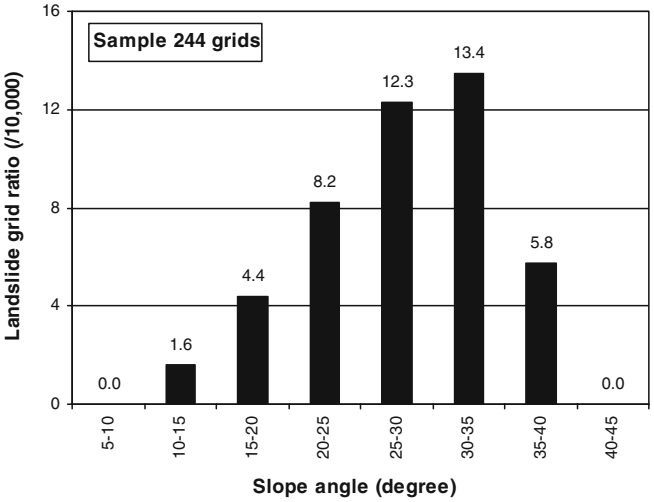

Fig. 7 Landslide density (landslide grid ratio) with respect to slope classes. Because dividing the number of landslide cells in a slope category by the total number of cells in that category, yields extremely small numbers we multiplied the ratio by 10,000

Location error evaluation of Digital Elevation Model on Google™ Earth

To investigate the slope angles of mapped landslides, it would have been best to calculate directly from GE, but GE gave neither a slope-calculation function nor DEM source information. Assuming that the slope angles calculated from the SRTM3-DEM were accurate, we estimated the location error of the DEM provided by GE.

Distinguished landmarks such as the confluences and meanders of rivers and summits of mountain peaks were selected. These points could be identified on both the GE and the SRTM3-DEM. Both GE and SRTM3-DEM use WGS84 ellipsoid to project locations (Google Earth 2008; NASA 2006). Nineteen points were selected as shown in Table 1. Longitude and latitude of these points were independently read from GE and from the SRTM3-DEM using ArcGIS 9.2. The location errors, i.e., discrepancy of the length between the same points on the GE and the SRTM3-DEM, were measured in meters, after projecting the UTM-zone 48N on the WGS84 ellipsoid. From these measurements, an average location error was found to be 146.5 m (Table 1) with a standard deviation of 105.1 m.

Terra ETL (2007) infers that GE projects longitude and latitude coordinates on computer screens not by a WGS84 ellipsoid but by a sphere so that these coordinates on the sphere are treated as if they were on the WGS84 ellipsoid (Přidal 2008). Neilsen (2008) stated that it causes position errors of up to 800 m. In Table 1 GE-DEM has the systematic location error of northwest direction to SRTM-DEM. Here, we cannot confirm whether the spherical projection error causes the 146.5 m error (Table 1) or not; however, we thought that this location error is independent of location error of FORMOSAT-2 image provided by GE, as explained in the following section.

Figure 6 shows location-error frequency. As shown in Fig. 6, error frequency of the class 45–90 m is highest; low error frequency dominates the higher error classes of 270–405 m. Because the DEM on GE is coarser than that of SRTM3-DEM, it was difficult to precisely locate some broad summits on GE. Such summits are codes 5–7 in Table 1. After eliminating these data, the average location error was found to be 107.9 m. This error is tolerated to view the landslides locations on GE; however, when we overlay them on SRTM3-DEM we cannot directly calculate statistics and we have to correctly process this error as explained hereafter.

Location error evaluation of FORMOSAT-2 image provided by GE

GE also published a SPOT5 image taken before the earthquake, which is geo-rectified to fit the DEM. In the study area, the SPOT5 image was taken on 10 November 2006 with an off nadir angle of 28.76°, according to SPOT images browsing system (http://sirius.spotimage.fr/). Figure 4b shows SPOT5's bird-eye view from south to north. As shown in Fig. 4c, an oblique aerial view from south to north, the FORMOSAT-2 image by GE is rectified to fit the map but less precisely. We think there are two reasons for this. It is thought that (1) the FORMOSAT-2 image was not orthorectified using a DEM, different from the SPOT5 image and that (2) the off nadir angle is larger in FORMOSAT-2 image than in the SPOT5 image. The numbered locations in Fig. 4b and c indicate the same points on the two images. Because of location errors, slopes calculated for the same points in the two images can be significantly different.

To calculate the correct slope angle of the landslides, it was also necessary to evaluate the FORMOSAT-2 image-location error. Ten landmarks were selected where they were clearly identified both on FORMOSAT-2 and SPOT5 images. Locations measured on the SPOT5 image are assumed to be correct. Distances between the same landmarks of FORMOSAT-2 and SPOT5 images were measured using GE. Table 2 shows the average distance (or error) was 1,038.6 m. The orthorectified SPOT5 image does not always indicate correct locations because the study area contains mountainous topography with large local relief; the accuracy of the orthorectified image is dependent on the quality of DEM and ground control points. However, because SPOT IMAGE (2005) stated that the obtained orthorectified image makes it possible to attain a 10-m-location accuracy (one sigma standard deviation), we thought that the SPOT5-location accuracy in the study area was negligible when compared to the 1,038.6 m discrepancy between the two imageries. This 1,038.6 m discrepancy shows that, even if landslide source is plotted carefully on the FORMOSAT-2 image,

the location may have a location error of about 1.0 km. This is because slope-tilt effect was not removed from FORMOSAT-2 image by GE, and this error does not include the location accuracy of the original FORMOSAT-2 image itself.

Estimating landslide slope angles

As a result of error evaluations, we found that we could not directly use slope angles overlain on the mapped landslide plots. To estimate the slope angles on the mapped landslides, slope angles were calculated from the SRTM3-DEM, and slope-angle data were grouped in 5° intervals (Fig. 7). The lowest class (0–5°) was eliminated because we know that all landslides occurred on much steeper mountain slopes. Slope data were classified into 15 classes from 5° to 80°. Since 13 landslides were located within the no-data area of SRTM3-DEM, we eliminated them. We drew a 1,044-m-radius circle centered on each landslide source; the 1,044 m was calculated using the error propagation law with 107.9 m (GE DEM location error) and 1,038.6 m (FORMOSAT-2 image location error). We searched for the most frequent slope-angle class in each circle and assigned the class to the respective landslides. Therefore, one pixel of the DEM was assigned to each landslide.

To normalize slope-angle frequency of the landslides, the frequency was divided by the area (the number of DEM pixels) within each slope-angle class. As a result, landslide density (landslide grid ratio) was obtained, as shown in Fig. 7, which indicates that the landslide density increases with slope up to 35°, above which the normalized frequency drops. This tendency has been already reported by many previous earthquake studies (e.g., Parise and Jibson 2000). To obtain more precise slope angles, it is necessary to use accurately geo-rectified satellite images with a DEM of higher resolution.

Conclusion and final remarks

To rapidly evaluate the distribution of landslides triggered by the 12 May 2008, Wenchuan earthquake, we used GE as a base map. As a result, 257 large landslides were identified and their locations plotted. It was found that the landslides were concentrated along the Beichuan fault and that the maximum spatial density of large landslides was 0.3 landslides/km^2. We used 8-m resolution FORMOSAT-2 imagery, but are certain that the number and density of observed landslides will increase if higher resolution imagery is used. The location error of GE DEM and FORMOSAT-2 image was estimated at 107.9 m and 1,038.6 m, and a total error of 1,044.6 m was estimated as the landslide mapping location accuracy. Using a sampling radius of 1,044 m, we found that the largest density of landslides occurred on slopes of 30–35°. Slope-angle frequency plots indicate that the steeper the slope angle, the higher the landslide frequency, and that landslide density drop at steeper slope angles.

Acknowledgements

Support for Hiroshi P. Sato's research at the U.S. Geological Survey facilities in Golden, CO was provided by a grant from the Ministry of Education, Culture, Sports, Science and Technology of Japan.

References

Colesanti C, Wasowski J (2006) Investigating landslides with space-borne Synthetic Aperture Radar (SAR) interferometry. Eng Geol 88:173–199, doi:10.1016/j.enggeo.2006.09.013

Dai FC, Lee CF, Deng JH, Tham LG (2005) The 1786 earthquake-triggered landslide dam and subsequent dam-break flood on the Dadu River, southwestern China. Geomorphology 65:205–221, doi:10.1016/j.geomorph.2004.08.011

Densmore AL, Ellis MA, Li Y, Zhou R, Hancock GS, Richardson N (2007) Active tectonics of the Beichuan and Pengguan faults at the eastern margin of the Tibetan Plateau. Tectonics 26(4):1–17, doi:10.1029/2006TC001987

Dong S, Zhang Y, Wu Z, Yang N, Ma Y, Shi W, Chen Z, Long C, An M (2008) Surface rupture and co-seismic displacement produced by the Ms8.0 Wenchuan earthquake of May 12th, 2008, Sichuan, China: eastwards growth of the Qinghai-Tibet Plateau. Acta Geol Sin 82(5):938–948

Geographical Survey Institute (2008) Crustal Deformation and Source Fault of the Sichuan (Wenchuan) Earthquake in 2008 (in Japanese). http://cais.gsi.go.jp/Research/topics/topic080604/index.html

Google Earth (2008) http://earth.google.com/userguide/v4/ug_importdata.html#note

Přidal KP (2008) http://www.maptiler.org/google-maps-coordinates-tile-bounds-projection/globalmaptiles.py

Neilsen MO (2008) http://www.sharpgis.net/author/Morten.aspx

NASA (2006) ftp://e0srp01u.ecs.nasa.gov/srtm

Parise M, Jibson RW (2000) A seismic landslide susceptibility rating of geologic units based on analysis of characteristics of landslides triggered by the 17 January, 1994 Northridge, California earthquake. Eng Geol 58:251–270, doi:10.1016/S0013-7952(00)00038-7

Sato HP, Hasegawa H, Fujiwara S, Tobita M, Koarai M, Une H, Iwahashi J (2007) Interpretation of landslide distribution triggered by the 2005 Northern Pakistan earthquake using SPOT 5 image. Landslides 4:113–122, doi:10.1007/s10346-006-0069-5

Science Museum of China (2008) Earthquake ruins in Diexi. http://www.kepu.net.cn/english/quake/ruins/rns16.html

SPOT IMAGE (2005) Preprocessing levels and location accuracy. http://www.spot.com/automne_modules_files/standard/public/p449_c868d036b7d60e9be17d5ea3c7930165-Processing_Levels_and_Accuracy.pdf

Taiwan National Space Organization (2008) FORMOSAT-2 features. http://www.nspo.org.tw/2005e/imagesell/SATproperty.htm

Tang B, Liu S, Liu S (1994) Mountain disaster formation in northwest Sichuan. GeoJournal 34:41–46, doi:10.1007/BF00813968

Terra ETL (2007) http://terraetl.blogspot.com/2007/10/google-maps-is-earth-sphere-or.html

Tobita M, Yarai H, Nishimura T, SAR team in GSI (2008) SAR-derived deformation fields and a fault model of the 2008 Wenchuan earthquake. U.S. Geological Survey Open-File Report 2008-1335:48–49. http://pubs.usgs.gov/of/2008/1335/of2008-1335.pdf

Une H, Kumaki Y (2007) "Remotely sensed" surface fault rupture accompanied with the northern Pakistan earthquake. E-Journal Geo 2:86–94, http://www.soc.nii.ac.jp/ajg/ejgeo/228694une.pdf (in Japanese with English abstract)

USGS (2008) Magnitude 7.9—EASTERN SICHUAN, CHINA. http://earthquake.usgs.gov/eqcenter/eqinthenews/2008/us2008ryan/

Xinhua (2008) At least 1,000 students buried in China county worst hit by quake. http://news.xinhuanet.com/english/2008-05/13/content_8157648.htm

H. P. Sato (✉)
Geography and Crustal Dynamics Research Center, Geographical Survey Institute, Tsukuba 305-0811, Japan
e-mail: hsato@gsi.go.jp

E. L. Harp
United States Geological Survey,
Box 25046MS 966, Denver Federal Center,
Denver, CO, USA